




Impact of Er addition on the electrical, optical, and transmittance characteristics of 0.91KNN–0.09SMT ferroelectric ceramics

Liwen Wang¹, Jiangting Wang¹, Kaishuo Liu¹, Chengjian Yu¹, Hua Wang^{1,2,*} , Jiwen Xu^{1,2}, Ling Yang¹, and Wei Qiu¹

¹School of Materials Science and Engineering, Guilin University of Electronic Technology, Guilin 541004, People's Republic of China

²Guangxi Key Laboratory of Information Materials, Guilin University of Electronic Technology, Guilin 541004, People's Republic of China

Received: 19 February 2023

Accepted: 11 April 2023

Published online:
25 April 2023

© The Author(s), under exclusive licence to Springer Science+Business Media, LLC, part of Springer Nature 2023

ABSTRACT

Er-doped 0.91(K_{0.5}Na_{0.5})NbO₃–0.09Sr(Mg_{0.5}Ta_{0.5})O₃ transparent fluorescent ceramics were prepared according to the traditional solid-phase method. The (K_{0.5}Na_{0.5})NbO₃ (KNN) ceramics were modified by introducing the second group elements Sr(Mg_{0.5}Ta_{0.5})O₃ and the rare-earth ions Er³⁺. Transparent ceramics' structural, optical, and electrical characteristics as a result of the effects of Er³⁺, investigations were done using 0.91KNN–0.09SMT: γ wt% Er. Results show that the representative 0.91KNN–0.09SMT: 0.1 wt% Er ceramics sample has a light transmittance of 60% in the near infrared (1000 nm) band, and the optical band gap (E_g) is found to be 2.62 eV. Phase structure analysis has revealed that the doping of Er³⁺ does not alter the structure of the ceramic's pseudo-cube phase. Er-doped KNN-SMT ceramics exhibit better up-conversion luminescence properties and also retain electrical properties. The Er³⁺ makes the doped ceramics have luminescence properties upconverting. With the increase of doping amount, the luminescence intensity of ceramics increases gradually at first and then decreases. Moreover, the ceramic also has some features for energy storage.

1 Introduction

Ceramics that are transparent exhibit outstanding chemical, mechanical and thermal stability [1–3]. As technology developed, some materials, such as sapphire for IR Windows, YAG (Yttrium aluminum garnet) for lasers, PZN-PT, and PbZn_{1/3}Nb_{2/3}O₃–

PbTiO₃ for photoelectric purposes, have been developed as single crystals [4, 5]. Technically speaking, these single crystals pose a challenge to manufacture, which is the main factor preventing their use in mass production, it's critical to develop low-cost processes for producing transparent ceramics with suitable mechanical and optical qualities [6, 7].

Address correspondence to E-mail: wh65@tom.com

Transparent pulse capacitors, sensors, storage, and transparent electronic components are all applications for transparent ferroelectric ceramics, a type of photoelectric ceramic that has exceptional optical and electrical properties [8–11].

Lead zirconate titanate (PZT) and La-doped lead zirconate titanate (PLZT) are transparent ferroelectric ceramic materials, which are commonly used in transparent ferroelectric ceramics, have large piezoelectric constants, electromechanical coupling coefficients, and outstanding photoelectric performance [2, 12, 13]. However, the use of lead-based ferroelectric materials has been restricted or outlawed in many nations due to the dangers they pose to the environment and public health, as a result, lead-free ferroelectric materials have been the focus of studies on rare-earth luminescence [14, 15]. Due to their large Piezoelectric constant and high Critical temperature, lead zirconate titanate (PZT) ferroelectric materials have been replaced by (K, Na)NbO₃ (KNN)-based ceramics, which have received extensive study as lead-free piezoelectric systems [16–22].

Potassium niobate K_{0.5}Na_{0.5}NbO₃ (KNN) is the prototypical ferroelectric transition metal base material without lead, is a solid solution with an A¹⁺B⁵⁺O₃²⁺ perovskite structure of KNbO₃ ferroelectric and NaNbO₃ antiferroelectric in a ratio of 1:1. The ferroelectric and piezoelectric capabilities of the KNN's ABO₃-type structure are good [23, 24]. Divalent ion Doping can affect how ceramic grains form and improve density, modify the phase structure, and enhance the electrical properties of ceramic samples by doping Sr²⁺ (R = 0.144 nm, CN = 12) in the A and B positions of the second component of KNN ceramics [1, 25, 26]. Doped Mg²⁺ can obviously improve the optical electric conductivity [27, 28], doping Ta⁵⁺ makes dense ceramic, ferroelectric, piezoelectric, improved [29]. In order to attain high transparency, ferroelectric ceramics can have their grain polished, their porosity decreased, and their density raised with the addition of rare-earth ions (Re³⁺) [30]. In Sr₃-YLi(PO₄)₃F ceramics, co-doping of Ho³⁺ and Eu³⁺ can create deep traps that enhance the color contrast, Eu³⁺ doped KNN can create a deeper trap, enabling it to get a quicker response time and higher contrast in the color rendering [31, 32]. It is well-known that rare-earth elements are added to piezoelectric materials to enhance their electrical characteristics. These substances can also be utilized in luminous materials as active ions. Since rare-earth elements like Pr, Er, Eu,

and Ho-doped in KNN ceramics, they exhibit luminous qualities. Fluorescent transparent ceramics are fluorescent materials based on transparent ceramics that have been doped with various trace rare-earth elements to produce light that emits various colors when excited by light, primarily up-conversion (UC) and down-conversion (DC) luminescence [3, 33–35]. Under the excitation of lower energy long wave, the emission of higher energy short-wavelength light, with this property of materials are called up-conversion luminescent materials [36]. The up-conversion luminous materials provide high conversion efficiency, great absorption capacity, and stable physical and chemical properties [37, 38]. The choice of substrate material is very important, because the luminescence efficiency of up-conversion luminescent material is mainly affected by the crystal structure and anion of substrate material, and the coordination number, ion spacing and spatial structure position also affect the crystal structure [39]. The matrix of up-conversion luminescent materials is mainly sulfide, fluoride, halide, oxide and fluorine oxide materials. Among these, the oxide exhibits strong temperature resistance and, for the most part, relatively stable properties. When rare-earth oxides are properly doped, they can increase the luminous intensity of ceramics, and rare-earth ions' distinct energy level structures can provide optical characteristics [40]. The rare-earth doping type and lattice matching of the substrate material are also important. Appropriate radius of doped with rareearth ions also has the characteristics of the low phonon energy, lower phonon energy can improve the luminous efficiency. In conclusion, to improve luminescence characteristics to a greater extent, it is necessary to get closer to the rule of rare-earth doping [41]. Up-conversion luminescent materials have promising applications in optical disc technology, information processing, medical diagnosis, optical fiber amplifier and anti-counterfeiting.

Sr(Mg_{1/3}Ta_{2/3})O₃ (SMT), the second component's solid solution greatly slows down grain growth in this study's experiment, causing the ceramic sample's grains to expand to nanoscale size and significantly enhancing the ceramic sample's transmittance [42]. Appropriate addition of Er³⁺ can also improve the luminescence and electrical properties of transparent KNN-SMT ceramics, which can be efficiently applied to high performance multifunctional optoelectronic devices. The traditional solid-phase sintering procedure was used to prepare Er-doped 0.91KNN–0.09SMT transparent ceramics.

Investigated were how Er³⁺ doping affected the ceramics' phase structure, transmittance, photoluminescence, and ferroelectric characteristics.

2 Experimental details

Using a traditional solid-phase approach, 0.91KNN–0.09SMT: *y* wt% Er (KNN–SMT: Er, *y* = 0.1, 0.2, 0.3, 0.4, 0.5, 0.6, 0.7, 0.8) was created. Anhydrous ethanol and ZrO₂ beads were used as the ball-milling medium in tanks that were filled with the feedstock, including K₂CO₃ (99.5%), Na₂CO₃ (99.8%), Nb₂O₅ (99.99%), SrCO₃ (99.9%), MgO (99.9%), Ta₂O₅ (99.9%), and Er₂O₃ (99.99%). To further mix the ingredients evenly, the powders were ball-milled for 12 h, calcined at 860 °C for 3 h, and then ball-milled again for 12 h to further mix the ingredients uniformly. Dried, thoroughly ground and sieved, to improve the fluidity of the powders, and then thoroughly agitated with polyvinyl alcohol with the mass fraction of 6 wt%. Once dried, completely ground and sieved, pressed into crude blanks of 12 mm diameter and 1 mm thickness under uniaxial pressure at 5 Mpa, and then maintained at 600 °C for 2 h to unload polyvinyl alcohol, and then sintered at 1170 °C for 3 h in order to fire the pellet body in the sintered ceramic sample, 0.3 mm of polishing was applied to the acquired samples.

X-ray diffractometer (XRD, D8 Advance, Bruker) determined the phases of the KNN-SMT: Er ceramics. The microstructure was viewed using a Field Emission scanning electron microscope (Quanta FEG-450, FEI Company, USA). UV–Vis spectrophotometer (UV-6100, Metash, China) measured the transmittance of light at 400–1000 nm from samples polished to a thickness of 0.3 mm. The ferroelectric system (TF Analyzer 2000HS, Germany) was used for testing of the hysteresis (*P*–*E*) buckles. Spectrophotometer (SENS-9000A, Zolix) conducted the measurement of fluorescence spectra under 980 nm excitation. The temperature-dependent dielectric properties were measured by a precision impedance analyzer (Agilent 4294A, USA).

3 Results and discussion

The optical transmittance spectra for Er-doped 0.91KNN–0.09SMT ceramics are displayed in Fig. 1a, ceramics Er-doped 0.91KNN–0.09SMT have a transparency of 44% to visible light (780 nm) and 60% to near

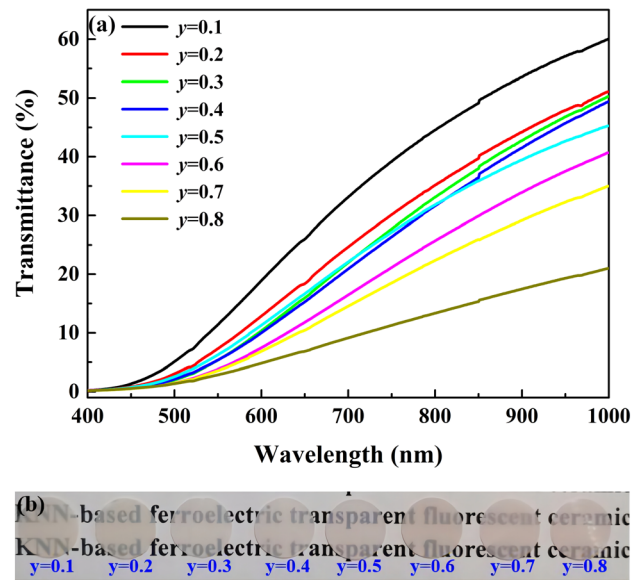


Fig. 1 a The variation curves of transmittance (%) with wavelength (nm) in the range 400–1000 nm. b Photograph of the KNN-SMT: Er transparent ceramics

infrared light (1000 nm) with an Er³⁺ doping concentration of 0.1 wt%, the ceramic has an extremely symmetric pseudo-cubic phase arrangement that renders it isotropic to light and lowers the quantity of light refraction at the grain frontiers. Er³⁺ doping changes the lattice of the ceramic, resulting in lattice expansion or contraction, affecting the symmetry of the ceramic structure. The interface reflection between the grains leads to serious loss of light intensity in the direction of light propagation. *y* = 0.6, the transmittance at 1000 nm is 40%; *y* > 0.8, the transmittance decreases to the minimum value, with the transmittance of 13% at 400 nm and 21% at 1000 nm. Therefore, the transmittance decreases with the increase of doping amount. In Fig. 1b shows the photographs of the ceramics (0.3 mm thickness), the lettering under the ceramics gradually blurs as the Er³⁺ content increases, which also indicates that the addition of rare-earth significantly reduces the transparency of the ceramics, especially when *y* > 0.6. The ceramic maintains its exceptional pellucidity despite the reduction in light transmission. Tauc equation can be used to determine the optical bandgap energy (*E_g*) from soaking up spectra, *E_g* is related to the absorption coefficient *α* as follows:

$$(\alpha h\nu)^2 = A(h\nu - E_g), \tag{1}$$

where *h* is Planck's constant and *ν* is the frequency of the photon, the constant *A*. In addition, using the transmittance *T*, *α* can be determined as follows:

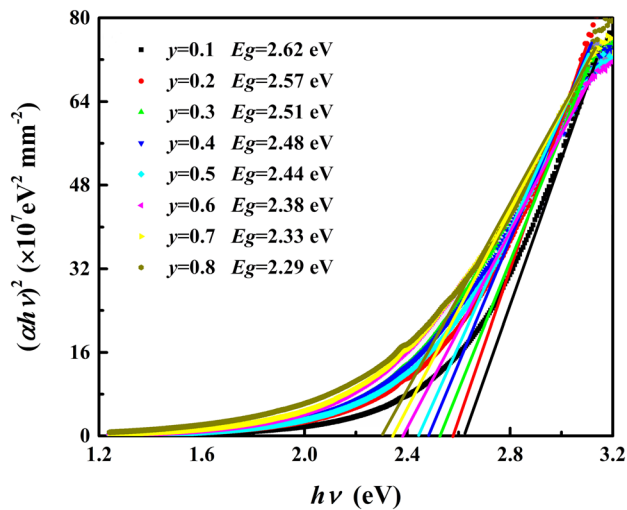


Fig. 2 Plots of $(\alpha hv)^2$ versus hv , energy band gap E_g for the Er-doped 0.91KNN-0.09SMT ceramics

$$\alpha = \frac{1}{t} \ln \frac{1}{T}, \quad (2)$$

where t is the thickness of each tested sample [43].

Based on the ceramics' ability to transmit light illustrated in Fig. 1a, calculated and displayed in Fig. 2 is the E_g of Er-doped 0.91KNN-0.09SMT ceramics. The E_g of ceramics Er-doped 0.91KNN-0.09SMT is 2.62 eV, comparable to the pure KNN ceramic's E_g of 2.63 eV. However, when $y = 0.8$, the E_g is decreased to 2.29 eV. The ion substitution in 0.91KNN-0.09SMT ceramics doped with Er changes the electron occupancy state of the ceramics. Due to the increase of Er, the original equilibrium state is broken, and the energy band of ceramics also changes. The electron transition must take in sufficient energy. When the band gap is larger, some electrons will be blocked from the transition behavior, so more energy will be used for optical transmission, thus reducing optical loss. The lower E_g is more likely to transfer electrons from valence bands than the higher E_g , conversely, uses less energy for optical transportation, thus leading to the decline of the light transmission ability of ceramics. It can be seen that the Er^{3+} can change the ceramic band gap, and that the E_g lowers as the Er^{3+} doping level rises, deteriorating ceramics' ability to transmit light.

The XRD patterns of the Er-doped 0.91KNN-0.09SMT ceramics in the 2θ range of 20° – 80° are displayed in Fig. 3a. Since the positions of all the peaks correspond to the standard map (PDF # 80-2497), and no impurity phases could be seen within the

detection resolution of the XRD analyzer. As a result, it may be assumed that the dopant ions Er^{3+} have spread into the crystal lattices and created a solid solution that was stable with 0.91KNN-0.09SMT. The XRD patterns in the range of 45° – 46.5° and Ta peaks above 60° were amplified to obtain greater peak details, as depicted in Fig. 3b and c, the fact that the diffraction peaks (200) and (220) do not split shows that the ceramics Er-doped 0.91KNN-0.09SMT preserves the pseudo-cubic phase's crystal structure.

In order to study the crystalline structure of the ceramics, the calculated lattice parameters of a , b , c , and the c/a ratio of the KNN-SMT: Er ceramics using the Jade 6.0 software package from the XRD data are provided in Table 1. When Er^{3+} ($R = 0.089$ nm, $\text{CN} = 12$) enters the lattice of 0.91KNN-0.09SMT ceramics, and the closest ion to it is Mg^{2+} ($R = 0.072$ nm, $\text{CN} = 6$), Ta^{5+} ($R = 0.064$ nm, $\text{CN} = 6$) and Nb^{5+} ($R = 0.064$ nm, $\text{CN} = 6$), the three ions undergo the swap and taking up the B-sites of the ceramic lattice, Er^{3+} has a slightly larger ionic radius, leading to the expansion of ceramic lattice, the diffraction peaks of XRD are shifted to a lower angle in the first instance. The amount of Mg^{2+} is minimal, and Ta^{5+} and Nb^{5+} will be substituted when the amount of Er^{3+} used for doping grows, the trivalent ions replace the pentavalent ions, increasing the anion gap, resulting in the shrinkage of the ceramic crystal lattice. Therefore, the Ta peak and (200) diffraction peak shift from low to high angle with the Er-doped.

To further investigate the effect of ion substitution in KNN-based crystals, Fig. 4a shows the Raman spectra of KNN-SMT: Er ceramics in the range of 100 to 900 cm^{-1} at room temperature. The Raman spectrum of KNN-based ceramics has 6 vibration modes: A_{1g} , E_g , $2F_{1u}$, F_{2g} and F_{2u} [44]. Peaks below 200 cm^{-1} can be attributed to the translation mode of Na^+/K^+ cations and rotation of the NbO_6 octahedron. The NbO_6 octahedron F_{2u} mode may also appear in this region, but its vibration is weak and almost flat with the baseline. The vibration mode F_{1u} below 300 cm^{-1} can be identified as the vibration of A-site ions. When $y = 0.1$, Raman spectra within the range of 500 – 650 cm^{-1} can fit two peaks, namely A_{1g} vibration mode near 612 cm^{-1} and $E_g(v_1)$ vibration mode near 555 cm^{-1} , however, due to the increase of Er doping amount, the acromial 515 cm^{-1} on the left side of v_1 began to protrude. In order to further study the changes in ceramic structure, the Gaussian fitting

Fig. 3 **a** XRD patterns of 0.91KNN–0.09SMT: *y* wt% Er ceramics; **b** Expansions in the 2θ range at 45°–46.5°; **c** Expansions in the 2θ range at 65°–68° of the Ta peak

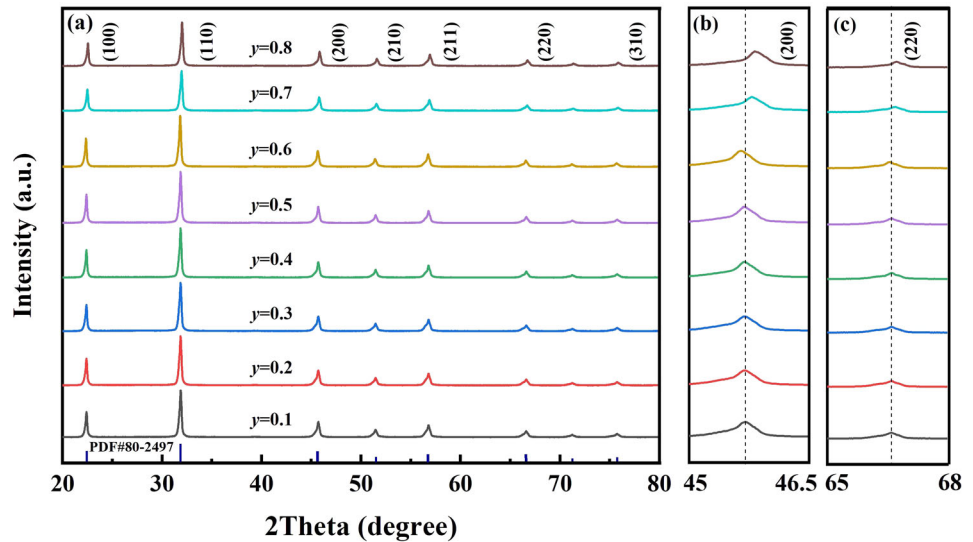


Table 1 The lattice parameters of 0.91KNN–0.09SMT: *y* wt% Er ceramics

<i>y</i>	<i>a</i> (Å)	<i>b</i> (Å)	<i>c</i> (Å)	<i>V</i> (Å ³)	<i>c/a</i>
0.1	3.9671	3.9677	3.9683	62.46	1.0003
0.2	3.9666	3.9676	3.9695	62.46	1.0007
0.3	3.9669	3.9677	3.9694	62.47	1.0006
0.4	3.9676	3.9680	3.9678	62.47	1.0001
0.5	3.9676	3.9677	3.9684	62.47	1.0002
0.6	3.9706	3.9701	3.9714	62.60	1.0002
0.7	3.9645	3.9617	3.9620	62.22	0.9994
0.8	3.9619	3.9590	3.9593	62.10	0.9993

method was used to fit the peaks at 500–650 cm⁻¹ in Fig. 4b. It can be seen that *v*₁ shifted to the low wavenumber. With the increase of Er²⁺ doping, the ion spacing inside the NbO₆ octahedron becomes longer and the interaction force decreases. When *y* = 0.6, the lattice cell volume reaches its maximum; when *y* > 0.6, *v*₁ value increases, which is because Er²⁺ starts to replace cations, shortening ion spacing between NbO₆ octahedrons, increasing bond energy, and strengthening ionic bond interaction. Figure 4c shows the Raman spectrum *v*₁ peak shift and FWHM of KNN–SMT: Er ceramics with different Er doping amounts. FWHM is the half-peak width of *v*₁. In KNN, the reduction of FWHM in *v*₁ mode is due to the migration of NbO₆ octahedron to low wavenumber, which weakens the interaction and effectively alleviates the lattice distortion. The characteristic peaks changed from flat at the beginning to sharp. Lattice defects caused by Er doping lead to the

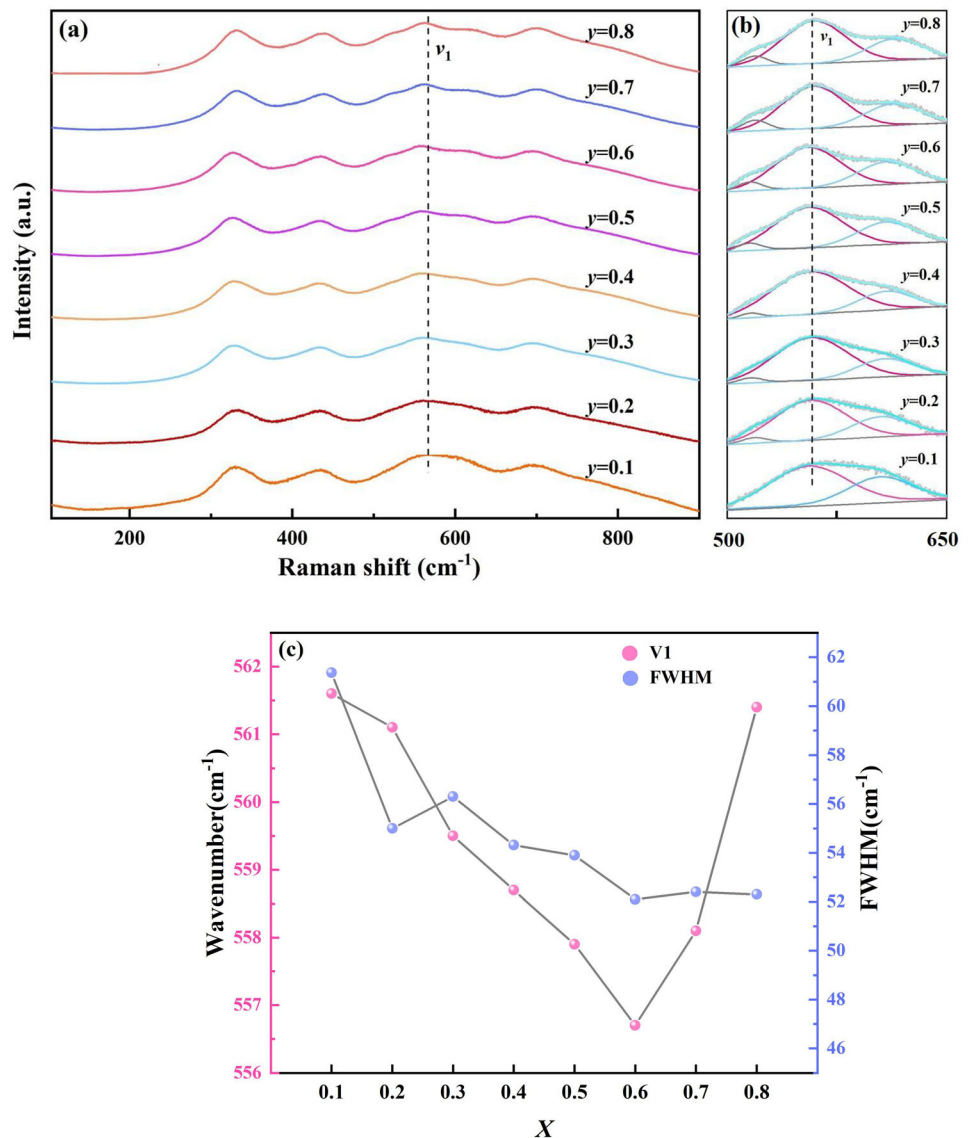
gradual sharpening of the two peaks on the left and right sides of *v*₁. Also due to the increase of impurity caused by doping, the ceramics turned to asymmetric structure.

Figure 5 presents SEM images of the Er-doped 0.91KNN–0.09SMT ceramics. The grains of the Er-doped 0.91KNN–0.09SMT ceramics grew very firmly and with a good compactness, which is why they all have good transparency, according to the morphologies of the samples on the free surface. Doping before and after Er³⁺, the grain shape differentiation of ceramics is not obvious, ceramics' grain morphology is fuzzily defined, which is primarily cubic grain. If the ceramic is over-doped with Er³⁺, the growth of the grains is slowed, a few tiny erratic-shaped particles appear on the surface, the grain boundaries blur, and the density of the ceramic decreases due to the microstructure. Figure 6 shows the effect of Er³⁺ doping amount on ceramic density. The ceramic density measurement formula is shown according to Eq. (3):

$$\rho = \frac{4m}{\pi d^2 h} \tag{3}$$

m is the quality of the ceramic; *h* is the thickness and *d* is the diameter. When *y* = 0.1, the density is 4.03 g/cm³, and as the Er doping amount increases; the density is 3.73 g/cm³ when *y* = 0.8. It can be seen that when more and more Er is added, the density of ceramics becomes lower and lower, showing an obvious downward trend. The rationale is that adding heterogeneous Er prevents densification, which causes the density to drop and, as a result, the light

Fig. 4 **a** Room-temperature Raman spectra of the 0.91KNN–0.09SMT: y wt% Er ceramics doped with various concentrations of erbium; **b** Expansions in the shifts at 500°–650°; **c** Line chart of ν_1 and FWHM that varies with the amount of erbium doped

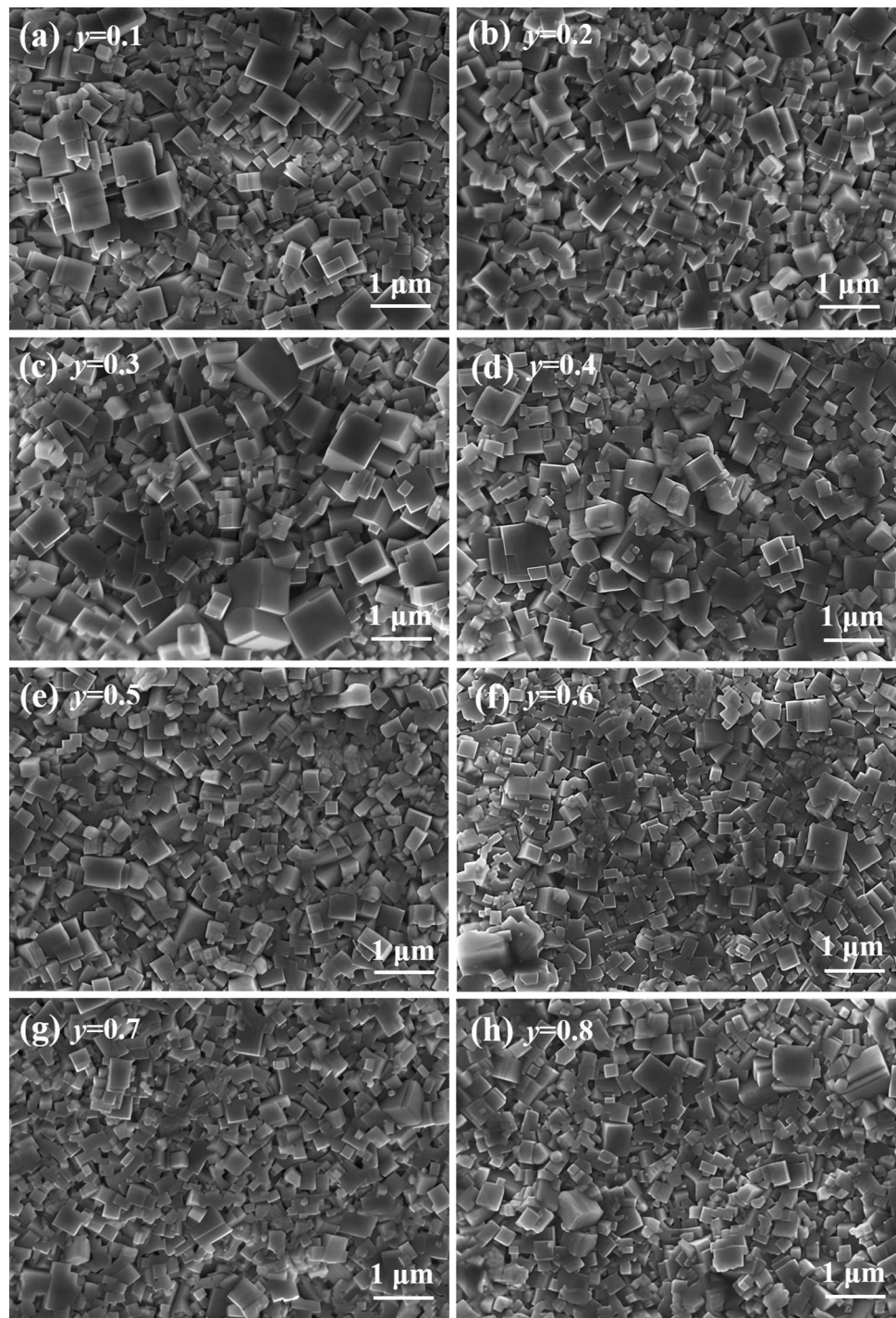


transmittance to drop. Moreover, the presence of uneven particles and pores will lead to the intensification of the scattering characteristics of light through transparent ceramics, weakening the ability of the ceramic to transmit light. As the doping quantity of Er^{3+} increases, the grain size distribution of the ceramics becomes progressively more concentrated. Both over-sized and undersized grains have decreased. The overall trend can also be exhibited in the line in Fig. 7a–i. In Fig. 7i, it can be seen from the SEM photographs that the formation of ceramic grain was aided by the trace Er^{3+} , where the average ceramic grain size increased from 0.174 to 0.193 μm from $y = 0.2$ to 0.3. In ceramics, sufficient Er^{3+} doping results in the emergence of widely spaced grain

boundaries, which will impede grain growth. When $y > 0.3$, which decreases from 0.193 to 0.133 μm for KNN–SMT: Er. Due to the fact that the grain size is much lower than the visible light wavelength (400–900 nm), the optical transparency of the KNN–SMT: Er ceramic is greatly enhanced from $y < 30\%$ to $y > 50\%$. In summary, the main factors contributing to the drop in the transmittance of ceramics are the establishment of more grain boundaries, the decline in density, and the continual reduction of grain size.

In Fig. 8a, the P – E hysteresis loops of KNN–SMT ceramics doped with different amounts of Er^{3+} obtained at the same electric field of 80 kV/cm. As can be seen, the electric hysteresis loop in the figure is characterized by “slender”, which is consistent with

Fig. 5 a–h SEM morphologies of the KNN–SMT: Er ceramics



the curve characteristics of relaxation ferroelectric materials and has high energy-storage efficiency. All Er-doped KNN-SMT ceramics exhibit P - E loops at saturation, it can be seen that after Er^{3+} doping, the ceramic P - E loops become narrower and it is seen that the rectangularity gradually decreases, indicating that Er^{3+} diminishes the ferroelectric property

and enhances the relaxation property of the ceramics. Er^{3+} has the potential to fine-tune ceramic grains. Larger grain boundaries will restrict the mobility of domain walls, which also degrades the ceramics' ferroelectric properties. The maximum and residual polarization intensities P_m and P_r of ceramics continuously decrease as the amount of Er^{3+} doping

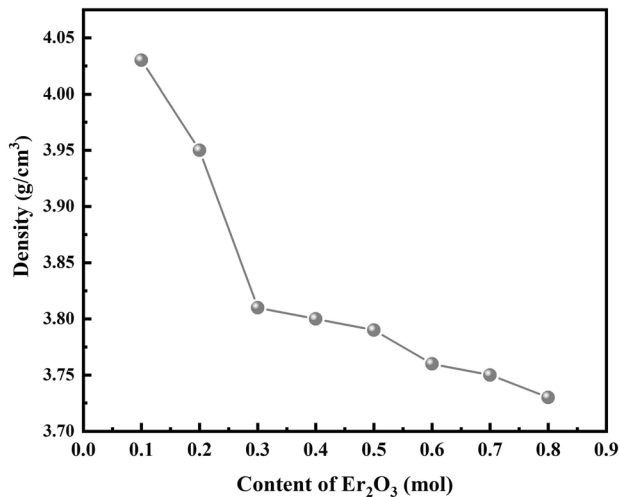


Fig. 6 Line chart of the density change of KNN-SMT: Er ceramics with different erbium doping amounts

increases. The fluctuation of ceramics' polarization intensity with increasing Er³⁺ doping levels is depicted in Fig. 8b. The graphic shows that the P_m and P_r both significantly dropped, the doping quantity rose from $y = 0.1$ to 0.2 , causing the values of 16.4 C/cm^2 and 2.89 C/cm^2 to decrease to 12.6 C/cm^2 and 1.54 C/cm^2 , respectively. Polarization gradually decreases and follows a similar changing trend after $y \geq 0.3$. Figure 8a shows that the small coercive electric field E_c and the existence of polar nano regions makes the P - E loops became slimmer, because of the narrow P - E loops lead to less energy loss, which demonstrated the superior stability of energy-storage for KNN-SMT: Er ceramics. Using Eq. (4), it is possible to determine the ferroelectric ceramic's energy-storage density W based on the P - E hysteresis loops:

$$W = \int_0^{P_m} EdP, \quad (4)$$

where P refers to the polarization and E to the electric field, following Eq. (5) can be used to calculate the recoverable energy-storage density W_{rec} :

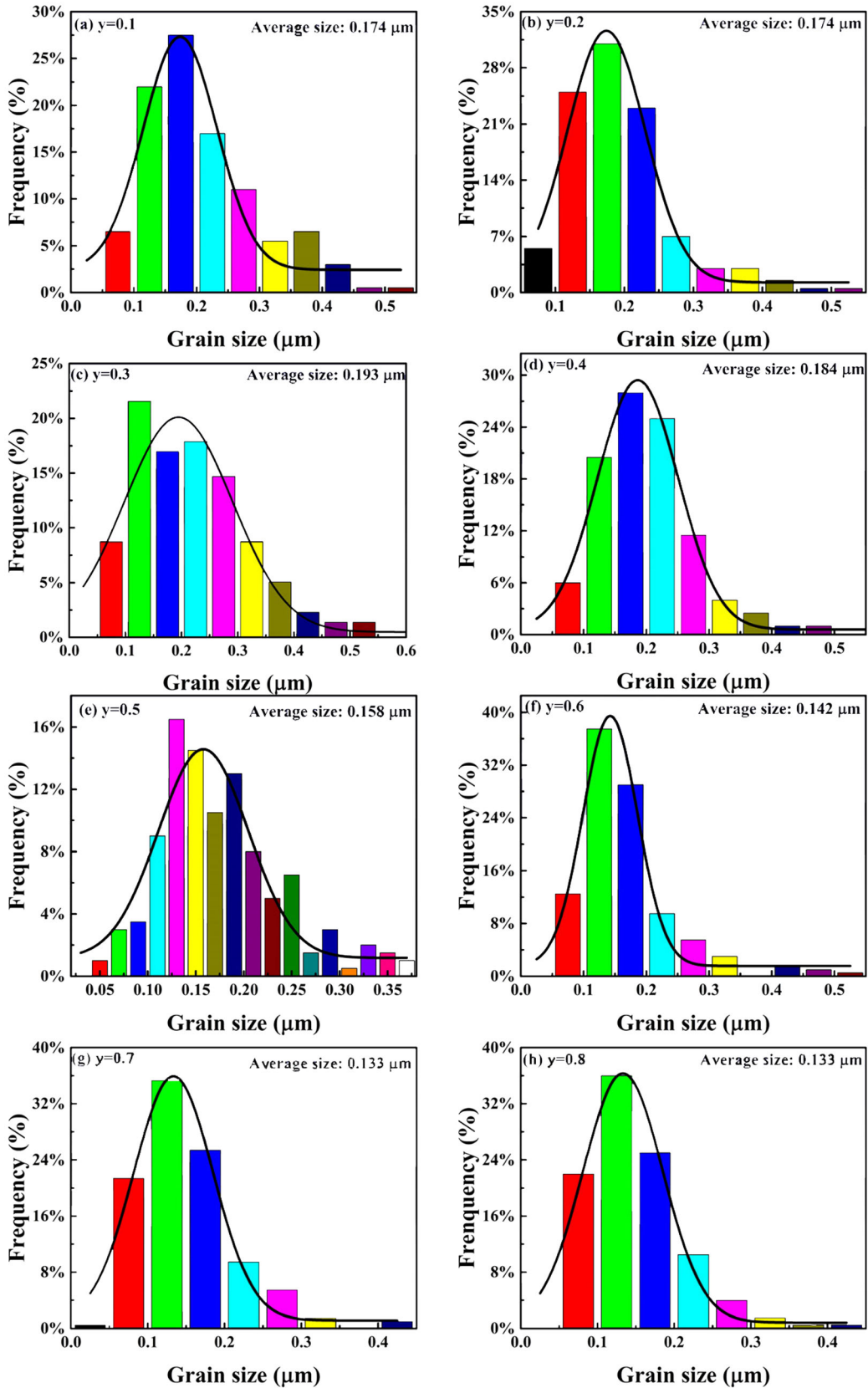
$$W_{rec} = \int_{P_r}^{P_m} EdP \quad (5)$$

Energy-storage efficiency η is another important measure for evaluating how well materials store energy, and it may be computed using Eq. (6):

$$\eta = \frac{W_{rec}}{W} = \frac{W_{rec}}{W_{rec} + W_{loss}} \times 100\% \quad (6)$$

The W and W_{rec} values of the KNN-SMT: Er ceramic samples are determined to be less than the critical failure strength using the P - E hysteresis loops of the KNN-SMT: Er ceramic samples as well as the equations stated above. Studying the energy-storage capabilities of ceramic samples with varying Er³⁺ doping contents [42]. Figure 8b was used to represent the energy-storage property of KNN-SMT: Er ceramic. As Er³⁺ is added, W_{rec} becomes more like the ceramic polarization change rule and has a general declining tendency, where W_{rec} and η are the energy-storage density and efficiency, while for $y = 0.1$ and 0.20 , $W_{rec} = 0.75 \text{ J/cm}^3$, $\eta = 68.9\%$ and $W_{rec} = 0.45 \text{ J/cm}^3$, $\eta = 71.4\%$, respectively. At $y = 0.1$, the KNN-SMT: Er ceramic's energy-storage density maximum value is attained, and when $y = 0.2$, the KNN-SMT: Er ceramic's efficiency maximum value is attained.

The KNN-SMT-Er curves measured at 1 kHz, 10 kHz, and 100 kHz, respectively, and the permittivity and dielectric loss as a function of temperature are shown in Fig. 9, with the test temperature ranging from ambient temperature to $500 \text{ }^\circ\text{C}$, which shows the results of the experiment. The diagram shows that the ceramic dielectric peak T_m , which corresponds to the maximum dielectric constant ϵ_m , appears in the test temperature range. $y = 0.1$, Curie peak $T_m = 36.9 \text{ }^\circ\text{C}$, while the maximum ϵ_m to 1173, and the frequency dispersion, which is caused by the relaxation of ceramics. The position of T_m barely varies, which indicates that doping Er³⁺ has no discernible impact on the phase transition of ceramics and the phase transition temperature of various components is constant at roughly $46 \text{ }^\circ\text{C}$, with more Er³⁺ doping, ceramics' maximum dielectric constant varies. Due to the modest quantity of doping, ceramics' dielectric constants tend to increase, with $y = 0.2$ and $\epsilon_m = 1539$. When $y > 0.3$, the maximum dielectric constant continuously declines while the dielectric loss gradually rises. This phenomenon indicates that a large amount of Er³⁺ doping will weaken the dielectric characteristics of ceramics. Er³⁺ enters the lattice of KNN-SMT ceramics and replaces the ions at the B-site causing the ceramic lattice to expand. Subsequently, the stability of the octahedral structure of NbO₆ is destroyed by the oxygen vacancy created during the substitution of Ta⁵⁺ and Nb⁵⁺, the ceramic's crystal lattice contracts, which eventually



◀ **Fig. 7 a–h** The average grain size distribution of KNN–SMT: Er ceramics; **i** Trend of average grain size of KNN–SMT: Er ceramics with increasing Er^{3+} doping

causes its maximum dielectric constant to drop as the quantity of Er^{3+} doping increases. The relationship between dielectric constant and temperature obeys the following formula:

$$\frac{1}{\varepsilon_r} - \frac{1}{\varepsilon_m} = \frac{(T - T_m)^\gamma}{C_1}, \tag{7}$$

where C is a constant; ε_m is the dielectric constant at T_{mi} ; ε is the dielectric constant at $T > T_m$; γ is the dispersion index, which describes the degree of dispersion of ferroelectrics at $T > T_m$. The γ value can be obtained by linear fitting [45].

The ceramics' dispersion index was determined, and the findings are depicted in Fig. 10 to help further examine the cause of the frequency spread of the

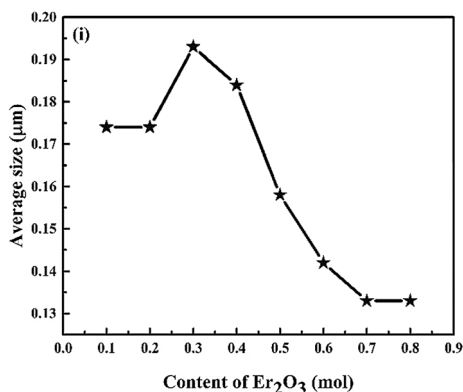


Fig. 7 continued

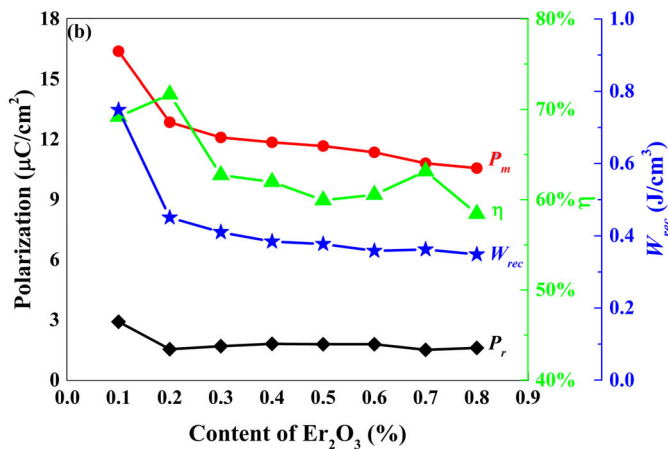
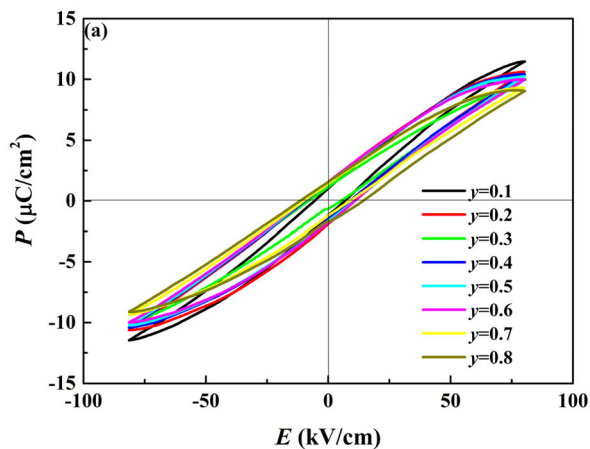


Fig. 8 a P – E loops at 80 kV/cm; **b** P_m , P_r , W_{rec} and η of KNN–SMT: Er ceramics

ceramic dielectric constant. This figure draws the test frequency of 1 kHz scatter plot and fitting a straight line, the slope of the straight line is γ . With γ value to determine the relaxation ferroelectrics [46]. The ion doping level increases, which causes the ceramic sample's crystal structure to expand and contract, distorting the local lattice and causing the polar nanoregion to form. This results in the ceramic sample's evident relaxation behavior. According to the results of the fitting, Er-doped 0.91KNN–0.09SMT ceramics can be considered to be a relaxation ferroelectric because the dispersion index values fall within the range of typical relaxor ferroelectrics.

The up-conversion emission spectra of the ceramics at 980 nm excitation are shown in Fig. 11a, observe that the green and red emission bands are present in the spectrum, and that the brightness of the brilliant red peak is low, as can be seen in Fig. 11a after applying magnification. It is clear from Fig. 11b and the energy transition theory of ceramics up-conversion luminescence that the energy transitions of $^4\text{S}_{3/2} \rightarrow ^4\text{I}_{15/2}$ and $^4\text{F}_{9/2} \rightarrow ^4\text{I}_{15/2}$ are responsible for the emission peaks of ceramics at 550 nm and 655 nm, respectively. The emission peak shape of the ceramics remains unchanged, that is Stark splitting does not occur, indicating that the crystal field near Er^{3+} does not change during the phase transition of the ceramics. As the amount of Er^{3+} doping grows, the photoluminescence intensity of ceramics rises, then falls. As the degree of Er^{3+} doping is varied from $y = 0.1$ to 0.4, the light intensity of the ceramic samples between the two component dots increases. When $y = 0.4$, the emission intensity of green light of ceramic sample reaches the strongest, which is about

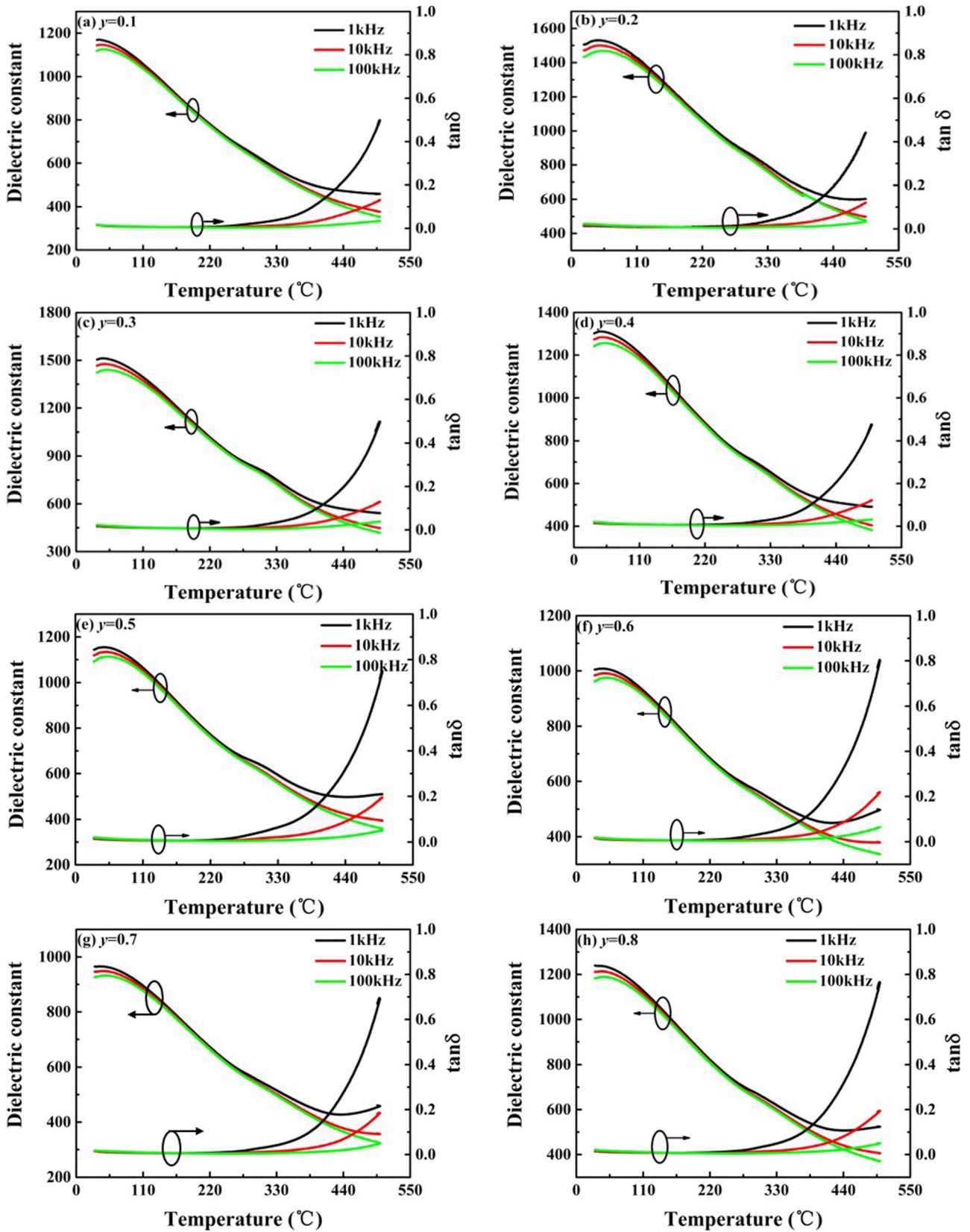


Fig. 9 a–h Temperature-dependent dielectric constant (ϵ_r) and loss ($\tan\delta$) of the KNN-SMT:Er ceramics

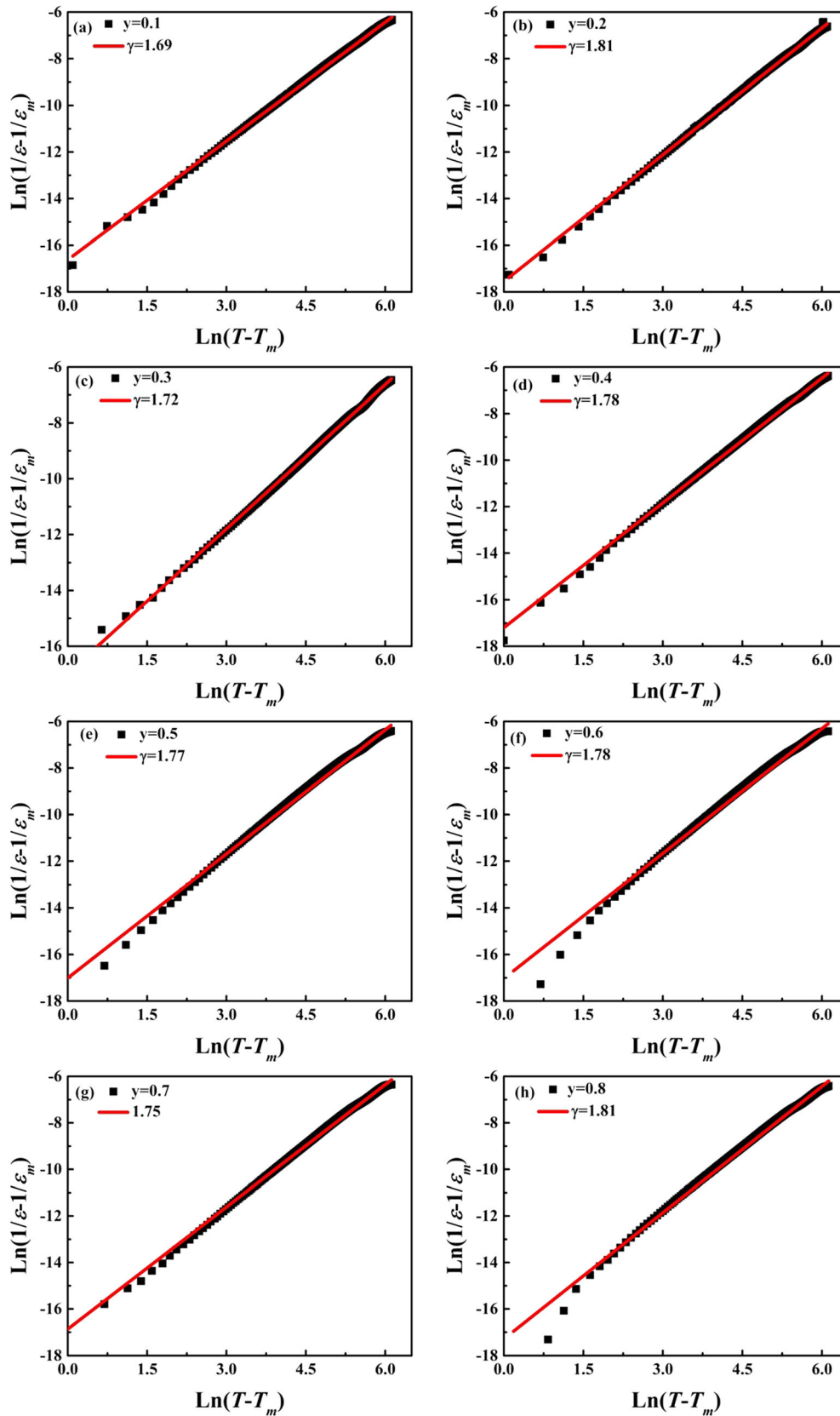


Fig. 10 a–h Dispersion index of 0.91KNN–0.09SMT: y wt% Er ceramics

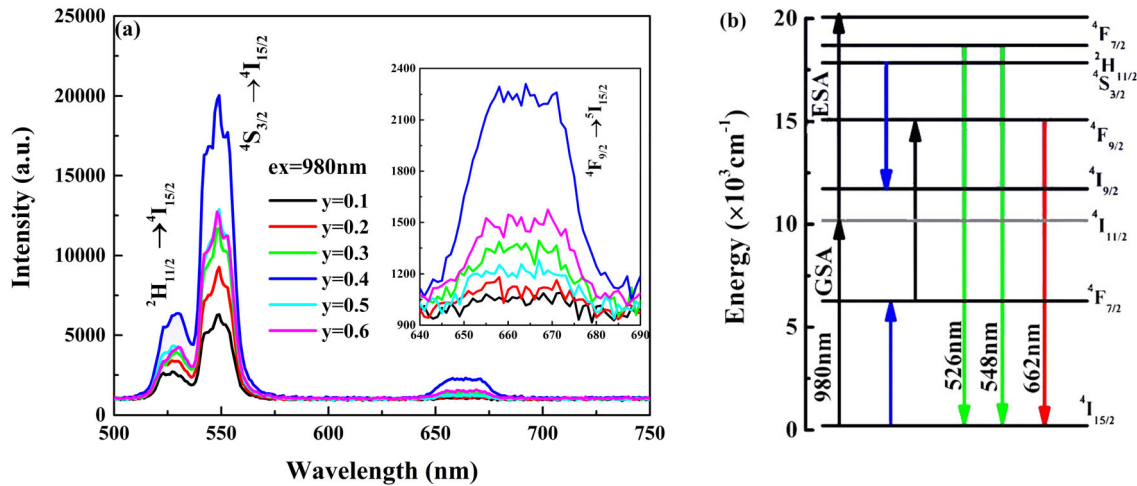


Fig. 11 **a** Up-conversion luminescence patterns of 0.91 KNN–0.09SMT: *y* wt% Er ceramics; **b** Schematic diagram of the up-conversion luminescence principle of Er³⁺ in ceramics

2×10^4 , but the emission intensity of red light is still quite feeble at this point. Because the symmetry of the position of Er³⁺ in Er-doped 0.91KNN–0.09SMT ceramics has a significant impact on the luminescence intensity of ceramics [47]. When Er³⁺ replaces Mg²⁺, Ta⁵⁺ and Nb⁵⁺, progressively lost the symmetry of the crystal structure, so the luminous intensity of ceramics starting to wane at *y* > 0.4, even *y* = 0.7 or 0.8, the samples already have difficulty exhibiting a typical conversion emission peak. Furthermore, the up-conversion luminescence intensity of the ceramics is also affected by the crystal defects; the presence of a vacancy in the crystal can trap a photon, weakening the up-conversion emission intensity of the ceramic.

4 Conclusions

Using the traditional solid-phase approach to dope rare-earth Er³⁺ in KNN–SMT, up-conversion luminous transparent ferroelectric ceramics were created. The structure, transparency, up-conversion luminescence, and electrical characteristics of the ceramics are significantly impacted by Er³⁺ doping. With an increase in Er³⁺ doping, the transmittance considerably drops from *y* = 0.1 to *y* = 0.8, and at 1000 nm, it drops from 60 to 20%. The doping of Er³⁺ did not alter the ceramics' pseudo-cubic phase structure, which persisted when the maximum luminescence intensity of 2.0×10^4 was obtained at *y* = 0.4, but it did give the ceramics up-conversion luminescence

features. When *y* = 0.1, $W_{rec} = 0.75 \text{ J/cm}^3$; when *y* = 0.2, $\eta = 71.4\%$. Ceramics are relaxor ferroelectrics, it is a versatile optoelectronic material.

Author contributions

All authors jointly participated in the data collection and experimental program exploration. Data collection, analysis and initial manuscript were completed by first author: LW. Revision and refinement of the manuscript was performed by the corresponding author: HW and the manuscript was published with the consent of all authors.

Funding

This work is supported by the National Nature Science Foundation of China (61965007) and Guangxi Key Laboratory of Information Materials, (Guilin University of Electronic Technology), P. R. China (201007-Z).

Data availability

The available in the article are true and valid which are recognized by all authors.

Declarations

Competing interests The authors declare no competing interest.

References

- L.W. Wang, H.N. Liu, C.J. Yu, K.S. Liu, H. Wang, J.W. Xu, L. Yang, W. Qiu, High-transmittance $(K_{0.5}Na_{0.5})NbO_3$ ferroelectric ceramics modified by $Sr(Bi_{0.5}Ta_{0.5})O_3$. *J. Electron. Mater.* **52**, 1050–1056 (2023)
- S.F. Wang, J. Zhang, D.W. Luo, F. Gu, D.Y. Tang, Z.L. Dong, G.E.B. Tan, W.X. Que, T.S. Zhang, S. Li, L.B. Kong, Transparent ceramics: processing, materials and applications. *Prog. Solid State Chem.* **41**, 20–54 (2013)
- H.T. Wu, G.B. Hu, S.Y. Shi, X. Liu, H. Wang, J.W. Xu, L. Yang, W. Qiu, S.J. Zhou, Effect of Ho addition on the optical and electrical properties of 0.98KNN–0.02SYT ceramics. *J. Electron. Mater.* **51**, 831–837 (2022)
- H. Shahbazi, M. Tataei, M.H. Enayati, A. Shafeiey, M. Azizi, Structure-transmittance relationship in transparent ceramics. *J. Alloys Compd.* **785**, 260 (2019)
- S.D. Zhang, F.X. Sun, X.L. Xia, C. Sun, L.M. Ruan, Multi-layer-combination method to retrieve high-temperature spectral properties of C-plane sapphire. *J. Heat Mass Tran.* **121**, 1011–1020 (2018)
- A. Ikesue, Y.L. Aung, T. Kamimura, S. Honda, Y. Iwamoto, Composite laser ceramics by advanced bonding technology. *Materials.* **11**, 271 (2018)
- W.B. Liu, J. Li, B.X. Jiang, D. Zhang, Y.B. Pan, 2.44 KW laser output of Nd: YAG ceramic slab fabricated by a solid-state reactive sintering. *J. Alloys Compd.* **538**, 258–261 (2012)
- H.T. Wu, S.Y. Shi, X. Liu, H. Wang, J.W. Xu, L. Yang, W. Qiu, S.J. Zhou, The $Ba(Bi_{0.5}Ta_{0.5})O_3$ modified $(K_{0.5}Na_{0.5})NbO_3$ lead-free transparent ferroelectric ceramics with high transmittance and excellent energy storage performance. *J. Mater. Sci. Mater. Electron.* **33**, 16045–16055 (2022)
- Z.H. Xiao, S.J. Yu, Y.M. Li, S.C. Ruan, L.B. Kong, Q. Huang, Z.R. Huang, K. Zhou, H.B. Su, Z.J. Yao, W.X. Que, Y. Liu, T.S. Zhang, J. Wang, P. Liu, D.Y. Shen, A. Mathieu, J. Zhang, D.Y. Tang, Materials development and potential applications of transparent ceramics: A review. *Mater. Sci. Eng. R Rep.* **139**, 100518 (2020)
- L.Q. Xu, F. Chen, F. Jin, D. Lan, L.L. Qu, K.X. Zhang, Z.X. Zhang, G.Y. Gao, H.L. Huang, T. Li, F.P. Zhang, K. Wang, Z. Zhou, W.B. Wu, Tuning electrical properties and phase transitions through strain engineering in lead-free ferroelectric $K_{0.5}Na_{0.5}NbO_3$ -LiTaO₃-CaZrO₃ thin films. *Appl. Phys. Lett.* **115**, 202901 (2019)
- M. Zhang, H.B. Yang, D. Li, Y. Lin, Excellent energy density and power density achieved in $K_{0.5}Na_{0.5}NbO_3$ -based ceramics with high optical transparency. *J. Alloys Compd.* **829**, 154565 (2020)
- A. Presas, Y.Y. Luo, Z.W. Wang, D. Valentin, M. Egusquiza, A review of PZT patches applications in submerged systems. *Sensors.* **18**, 2251 (2018)
- Z.W. Xu, X. Zeng, Z.D. Cao, L. Ling, P.S. Qiu, X.Y. He, The electrical and optical properties of Nb-doping PLZT (9/65/35) transparent ceramics. *J. Electroceram.* **44**, 215–222 (2020)
- J.F. Lin, J.W. Zhai, X. Wu, B. Shen, H.H. Ye, H.J. Wang, Simultaneously improved transparency, photochromic contrast and Curie temperature via rare-earth ion modification in KNN-based ceramics. *Inorg. Chem. Front.* **8**, 2027 (2021)
- J.G. Wu, Perovskite lead-free piezoelectric ceramics. *J Appl Phys.* **127**, 190901 (2020)
- S.Y. Shi, G.B. Hu, M.C. Wang, H.T. Wu, X. Liu, H. Wang, J.W. Xu, L. Yang, W. Qiu, Introduction of $Sr(In_{0.5}Ta_{0.5})O_3$ to modulate phase structure and optoelectronic properties of $(K_{0.5}Na_{0.5})NbO_3$ ceramics. *J. Electron. Mater.* **51**, 6913–6920 (2022)
- G.B. Hu, H.N. Liu, J.T. Wang, Y.B. Sun, H. Wang, J.W. Xu, L. Yang, C.R. Zhou, Regulating the structural, transmittance, ferroelectric, and energy storage properties of $K_{0.5}Na_{0.5}NbO_3$ ceramics using $Sr(Yb_{0.5}Nb_{0.5})O_3$. *J. Electron. Mater.* **50**, 968–977 (2021)
- Y.F. Chang, Z.P. Yang, Y.T. Hou, Z.H. Liu, Z.L. Wang, Effects of Li content on the phase structure and electrical properties of lead-free $(K_{0.46-x/2}Na_{0.54-x/2}Li_x)(Nb_{0.76}Ta_{0.20}Sb_{0.04})O_3$ ceramics. *Appl. Phys. Lett.* **90**, 232905 (2007)
- M. Ichiki, L. Zhang, M. Tanaka, R. Maeda, Electrical properties of piezoelectric sodium-potassium niobate. *J. Eur. Ceram. Soc.* **24**, 1693–1697 (2004)
- J.F. Li, K. Wang, F.Y. Zhu, L.Q. Cheng, F.Z. Yao, (K, Na)NbO₃-based lead-free piezoceramics: fundamental aspects, processing technologies, and remaining challenges. *J. Am. Ceram. Soc.* **96**, 3677–3696 (2013)
- J. Rodel, W. Jo, K.T.P. Seifert, E.M. Anton, T. Granzow, D. Dam-Janovic, Perspective on the development of lead-free piezoceramics. *J. Am. Ceram. Soc.* **92**, 1153–1177 (2009)
- Y.B. Sun, H. Wang, G.B. Liu, H. Xie, C.R. Zhou, G.H. Chen, C.L. Yuan, J.W. Xu, High energy storage efficiency and high electrostrictive coefficients in BNT-BS-xBT ferroelectric ceramics. *J. Mater. Sci. Mater. Electron.* **31**, 5546–5553 (2020)
- J.T. Wang, Y.B. Sun, S.Y. Shi, H. Wang, J.W. Xu, L. Yang, W. Qiu, Effects of Er^{3+} doping on the structure and electro-

- optical properties of 0.94(K_{0.5}Na_{0.5})NbO₃-0.06Sr(Zn_{1/3}Nb_{2/3})O₃ ceramics. *Bull. Mater. Sci.* **45**, 14 (2022)
24. H. Wang, X.Y. Zhao, J.W. Xu, X. Zhai, L. Yang, Structure and properties of (1-x)[(K_{0.5}Na_{0.5})NbO₃-LiSbO₃]-xBiFe_{0.8}Co_{0.2}O₃ lead-free piezoelectric ceramics. *Bull. Mater. Sci.* **39**, 743–747 (2016)
 25. B.Y. Qu, H.L. Du, Z.T. Yang, Q.H. Liu, Large recoverable energy storage density and low sintering temperature in potassium-sodium niobate-based ceramics for multilayer pulsed power capacitors. *J. Am. Ceram. Soc.* **100**, 1517–1526 (2017)
 26. G.B. Hu, J.T. Wang, X. Liu, H.N. Liu, H. Wang, J.W. Xu, L. Yang, C.R. Zhou, W. Qiu, Structural, transmittance, ferroelectric, energy storage, and electrical properties of K_{0.5}Na_{0.5}NbO₃ ceramics regulated by Sr(Yb_{0.5}Ta_{0.5})O₃. *J. Mater. Sci. Mater. Electron.* **32**, 22300–22308 (2021)
 27. I. Blazquez-Alcover, G. Rousse, D. AlvesDallaCorte, J.C. Badot, A. Grimaud, P. Rozier, J.M. Tarascon, Improving ionic conductivity by Mg-doping of A₂SnO₃ (A=Li⁺, Na⁺). *Solid State Ion.* **308**, 16–21 (2017)
 28. S. Arif, N. Bano, M. Riaz, M.S. Anwar, Effect of magnesium substitution on structural and dielectric properties of 46.1SiO₂-26.9CaO-24.4Na₂O-2.6P₂O₅ ceramic. *Mater. Chem. Phys.* **281**, 125873 (2022)
 29. D.H. Zhang, Y.L. Zhang, S.H. Yang, Microstructure and electrical properties of tantalum doped (Ba_{0.85}Ca_{0.15})(Zr_{0.10}Ti_{0.90})O₃ ceramics. *J. Mater. Sci. Mater. Electron.* **26**, 909–915 (2015)
 30. J.F. Lin, Q.L. Lu, X. Wu, H.L. Sun, C. Lin, T.F. Lin, K.-H. Xue, X.S. Miao, B.S. Sa, Z.M. Sun, In situ boost and reversible modulation of dual-mode photoluminescence under an electric field in a tape-casting-based Er-doped K_{0.5}Na_{0.5}NbO₃ laminar ceramic. *J. Mater. Chem. C* **7**, 7885–7892 (2019)
 31. Y. Lv, Y.H. Jin, C.L. Wang, L. Chen, G.F. Ju, Y.H. Hu, Sr₃YLi(PO₄)₃F: Eu²⁺, Ln³⁺: colorless-magenta photochromism and coloration degree regulation through Ln³⁺ co-doping. *RSC Adv.* **7**, 43700–43707 (2017)
 32. Y. Zhou, P. Wang, J.F. Lin, Q.L. Lu, X. Wu, M. Gao, T.F. Lin, C. Lin, X.H. Zheng, High-contrast photochromic Eu-doped K_{0.5}Na_{0.5}NbO₃ ceramics with prominent Pellucidity. *Dalton Trans.* **50**, 4914–4922 (2021)
 33. Y.B. Sun, H. Wang, C.R. Zhou, L. Yang, J.W. Xu, Enhancement of the up-conversion luminescence performance of Ho³⁺-doped 0.825K_{0.5}Na_{0.5}NbO₃-0.175Sr(Yb_{0.5}Nb_{0.5})O₃ transparent ceramics by polarization. *Bull. Mater. Sci.* **44**, 139 (2021)
 34. J. Zhou, Q. Liu, W. Feng, Y. Sun, F.Y. Li, Up-conversion luminescent materials: advances and applications. *Chem. Rev.* **115**, 395–465 (2015)
 35. Y.T. Zhong, H.J. Dai, A mini-review on rare-earth down-conversion nanoparticles for NIR-II imaging of biological systems. *Nano Res.* **13**, 1281–1294 (2020)
 36. Z.B. Li, J.X. Yang, M. Shi, L. Yang, Y.P. Cheng, X.W. Hu, X.F. Jiang, X.B. Xing, S.L. He, Upconversion luminescence of graphene oxide through hybrid waveguide. *J. Phys. Chem. C.* **122**(29), 16866–16871 (2018)
 37. X. Liu, G.B. Hu, H.T. Wu, S.Y. Shi, H. Wang, J.W. Xu, L. Yang, W. Qiu, Transmittance, photoluminescence and electrical properties in Er-DOPED 0.98K_{0.5}Na_{0.5}NbO₃-0.02Sr(Yb_{0.5}Ta_{0.5})O₃ ferroelectric ceramics. *Ceram. J. Electron. Mater.* **51**, 3476–3484 (2022)
 38. T. Aitasalo, P. Dereń, J. Hölsä, H. Jungner, J.C. Krupa, M. Lastusaari, J. Legendziewicz, J. Niittykoski, W. Stręk, Persistent luminescence phenomena in materials doped with rare earth ions. *Solid State Chem.* **171**, 114–122 (2003)
 39. X.Q. Li, L.P. Lu, H.Y. Sun, X.Y. Zhang, Z.H. Bai, X.Y. Mi, Er³⁺, Yb³⁺ Co-doped Gd₂O₃S up-conversion phosphor: crystal structure, up-conversion luminescence and luminescence lifetime. *ECS J. Solid State Sci. Technol.* **9**, 106001 (2020)
 40. T.Y. Bian, T.H. Zhou, Y. Zhang, Preparation and applications of rare-earth-doped ferroelectric oxides. *Energies* **15**(22), 8442 (2022)
 41. Y.T. Huang, S.J. Zhuang, L.X. Peng, J.S. Wu, T.D. Liao, C.H. Xu, Y.F. Duan, Efficiency improvement of up-conversion luminescence of Yb³⁺/Tm³⁺ co-doped tellurite glass microsphere. *J. Alloys Compd.* **748**, 93–99 (2018)
 42. H.N. Liu, J.T. Wang, H. Wang, J.W. Xu, C.R. Zhou, W. Qiu, Er³⁺ and Sr(Bi_{0.5}Nb_{0.5})O₃-modified (K_{0.5}Na_{0.5})NbO₃: a new transparent fluorescent ferroelectric ceramic with high light transmittance and good luminescence performance. *Ceram. Int.* **48**, 4230–4237 (2022)
 43. X. Liu, H.T. Wu, S.Y. Shi, H. Wang, J.W. Xu, L. Yang, W. Qiu, Effects of Ba(Mg_{1/3}Ta_{2/3})O₃ doping on phase structure, optical and electrical properties of (K_{0.5}Na_{0.5})NbO₃ transparent ferroelectric ceramics. *J. Mater. Sci. Mater. Electron.* **33**, 22400–22409 (2022)
 44. X. Ren, Q. Chai, X. Zhao, Z. Peng, D. Wu, P. Liang, L. Wei, Z. Yang, X. Chao, Relaxor behaviors and electric response in transparent 0.95(K_{0.5}Na_{0.5}NbO₃)-0.05Ca(Zr_xZn_yNb_z)_{1.025}O₃ ceramics with low-symmetric structure. *Ceram. Int.* **45**, 3961–3968 (2019)
 45. J. Zhang, L. Yang, J.W. Xu, C.R. Zhou, C.L. Yuan, H. Wang, G.H. Rao, Photo-dielectric response enhancement and switching behavior of (1-x)(K_{0.5}Na_{0.5})NbO₃-xCa(Ni_{0.5}Nb_{0.5})O₃-δ ceramics by semiconduction method. *J. Alloys Compd.* **881**, 160512 (2021)
 46. X. Zhang, F. Yang, W.J. Miao, Z. Su, J.H. Zhao, L.M. Tang, Y.H. Shen, D. Hu, Y.Y. Chen, P. Li, J.J. Liu, Z.B. Pan, Effective improved energy storage performances of

- Na_{0.5}Bi_{0.5}TiO₃-based relaxor ferroelectrics ceramics by A/B-sites co-doping. *J. Alloys Compd.* **883**, 160837 (2021)
47. J. Wang, L.H. Luo, Y.P. Huang, W.P. Li, F.F. Wang, Strong correlation of the electrical properties, up-conversion photoluminescence, and phase structure in Er³⁺/Yb³⁺ co-doped (1-x)K_{0.5}Na_{0.5}NbO₃-xLiNbO₃ ceramics. *Appl. Phys. Lett.* **107**, 192901 (2015)

Publisher's Note Springer Nature remains neutral with regard to jurisdictional claims in published maps and institutional affiliations.

Springer Nature or its licensor (e.g. a society or other partner) holds exclusive rights to this article under a publishing agreement with the author(s) or other rightsholder(s); author self-archiving of the accepted manuscript version of this article is solely governed by the terms of such publishing agreement and applicable law.